

Microscopic Theory Revealing Dual Field-Induced Transitions in Spin- $\frac{1}{2}$ Screw-Chain Magnets

Mandev Bhullar,¹ Philip Richard,¹ and Hae-Young Kee^{1,2,*}

¹*Department of Physics, University of Toronto, Ontario, Canada M5S 1A7*

²*Canadian Institute for Advanced Research, CIFAR Program in Quantum Materials, Toronto, Ontario, Canada, M5G 1M1*
(Dated: December 11, 2025)

We develop a microscopic theory for pseudospin- $\frac{1}{2}$ screw-chain compounds with spin-orbit coupling that goes beyond the phenomenological site-dependent g -tensor description traditionally used for XXZ-like $\text{BaCo}_2\text{V}_2\text{O}_8$ and related materials. Starting from the symmetry-allowed $JK\Gamma$ Hamiltonian with Heisenberg J , Kitaev K , and off-diagonal Γ interactions, we show that the Γ interaction naturally generates the four-sublattice pattern associated with the crystal's screw symmetry. Using the density matrix renormalization group, we identify two distinct field-induced transitions. The first is a continuous transition into an intermediate phase, where the symmetry responsible for the two-fold ground-state degeneracy is broken. The second is a first-order transition into the high-field phase, characterized by a discontinuous jump in the spin-spin correlator. Entanglement-entropy scaling confirms that the first transition belongs to the Ising critical point with the central charge $1/2$. These results establish a microscopic framework for pseudospin- $\frac{1}{2}$ screw-chain systems such as Co^{2+} materials, uncover an intermediate phase whose width increases with Γ , and provide guidance for systematic exploration of additional field orientations and structural distortions.

Introduction - One-dimensional (1D) spin chains have attracted significant interest over recent years as they combine theoretical solvability, numerical accessibility and experimental relevance [1–6]. Among several extensively studied materials, one particular compound that has attracted a lot of attention is the quasi 1D-chain $\text{BaCo}_2\text{V}_2\text{O}_8$ [7–16], where Co^{2+} ions are arranged in screw chains running along the fourfold c -axis of a tetragonal structure [10, 11, 17–20], as shown in Fig. 1. It exhibits an antiferromagnetic (AFM) phase with strong Ising-like anisotropy in the absence of an external field [8], where the ordered magnetic moments are tilted away from the c -axis slightly by an angle ϕ [12, 15, 16, 19, 21, 22]. Under the [100] field direction, it was shown through thermal expansion and magnetostriction measurements that the canted AFM phase transitions to a disordered phase [12, 13, 19, 21, 23], as if it is well described by a collection of weakly coupled spin-1/2 XXZ chains with a dominant Ising interaction.

However, unusual spin excitations under a magnetic field have generated extensive studies beyond the XXZ model. A phenomenological anisotropic site-dependent g -tensor was employed to explain additional effective staggered fields perpendicular to both the transverse field and the Ising axis [12, 15, 16, 24]. Such g -tensor has been widely used so far and notably it was shown to display dual solitonic excitations below and above the critical field described by a dual-field double sine-Gordon model with a topological transition [15, 25, 26], sparking considerable excitement. However, a microscopic origin of the unusual site-dependent g -tensor has not yet been found, which hinders full exploration of field-induced phases.

Here, we address an origin of the site-dependent g -tensor via establishing the microscopic spin model, which

further allows to examine field-induced phases and their characters. We note that the Co^{2+} ion in $\text{BaCo}_2\text{V}_2\text{O}_8$ exhibits the $3d^7$ configuration with an effective pseudospin-1/2 due to spin-orbit coupling [27, 28]. Hence, a 1D version of the nearest neighbour (n.n.) exchange model known as the $JK\Gamma$ model, composed of Heisenberg (J), bond-dependent Kitaev (K), and Gamma (Γ) interactions, is expected [27, 29–33]. We show that the $JK\Gamma$ model provides the essential microscopic framework for understanding the ordered state and the transition under a field. The 1D chain $\text{BaCo}_2\text{V}_2\text{O}_8$ displays a dominant ferromagnetic (FM) Kitaev interaction with an AFM Heisenberg and a finite Γ interaction, which naturally leads to the site-dependent staggered field without an external field. We further show that what appears as a single transition is instead two closely-spaced transitions, where an intermediate region increases with the Γ interaction.

Microscopic Hamiltonian construction - To derive a microscopic theory for the $\text{BaCo}_2\text{V}_2\text{O}_8$ chain, we first recall the atomic wavefunction of Co^{2+} , which gives rise to pseudospin-1/2 through the interplay of Hund's coupling and spin-orbit coupling (SOC). A Co^{2+} ion with a $3d^7$ electron configuration surrounded by an octahedral cage of oxygen atoms generates a cubic crystal field that splits the d -orbital manifold into t_{2g} and e_g states, separated by an energy Δ_c . Due to a large Hund's coupling J_H ($J_H > \Delta_c$), the Co^{2+} ion forms a high-spin $t_{2g}^5 e_g^2$ electron configuration and a 12-fold degenerate $L = 1$, $S = 3/2$ subspace is further split by SOC resulting in a low-energy, pseudospin $J_{\text{eff}} = 1/2$ Kramer's doublet [27, 28, 30, 32].

The Co^{2+} ions form a four-fold screw chain rotating along the crystallographic c -axis, as shown in Fig. 1(a). They are linked by edge-sharing oxygen octahedra which define four local cartesian coordinate systems in a unit cell denoted by $(x_\alpha, y_\alpha, z_\alpha)$ with $\alpha = 1, 2, 3, 4$ representing repeating four-sites. Using this local coordinate sys-

* hy.kee@utoronto.ca

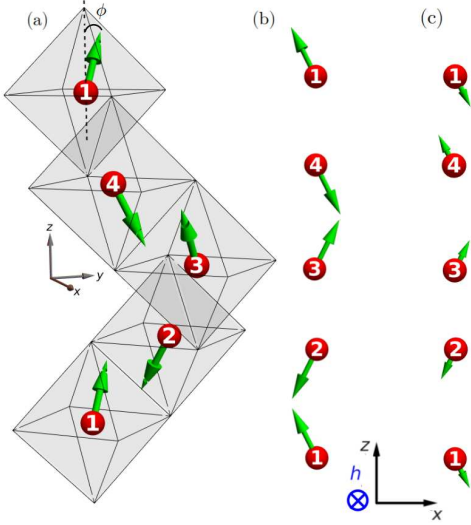


Fig. 1: (a) Structure of the Co²⁺ (red) screw chain with the zero-field moment directions (green). The xyz coordinate system is aligned with the crystallographic abc axes. $\alpha = 1, 2, 3, 4$, which denote the four sublattices, are shown in each octahedron. The green arrows represent the magnetic moments in the zx -plane under a magnetic field h applied along the y -axis for (b) $h < h_{c1}$ and (c) $h > h_{c2}$. Here, the length of the arrow and the tilt angle ϕ are exaggerated for visibility.

tem with ideal octahedra, the n.n. generic $J_{\text{eff}} = 1/2$ exchange model for each n.n. x- and y-bond going along the screw chain is given by the $JK\Gamma$ model [27–29, 32–35]

$$H_{\langle ij \rangle}^{\gamma} = J \mathbf{S}_i \cdot \mathbf{S}_j + K S_i^{\gamma} S_j^{\gamma} + (-1)^{\lfloor \frac{i-1}{2} \rfloor} \Gamma (S_i^{\beta} S_j^z + S_i^z S_j^{\beta}), \quad (1)$$

where $\gamma = x/y$ and $\beta = y/x$, respectively. The sign structure of Γ term stems from the $\pi/2$ rotation about the screw axis; the full derivation is given in the Supplementary Material (SM).

Including the four-sublattice dependence, the full Hamiltonian is given by

$$H = \sum_{j=1}^N \left\{ J \left[\epsilon (S_j^x S_{j+1}^x + S_j^y S_{j+1}^y) + S_j^z S_{j+1}^z \right] + \frac{K}{2} \left[(-1)^j (S_j^x S_{j+1}^x - S_j^y S_{j+1}^y) \right] - \Gamma \left[\cos \left(\frac{\pi j}{2} \right) (S_j^x S_{j+1}^z + S_j^z S_{j+1}^x) - \sin \left(\frac{\pi j}{2} \right) (S_j^y S_{j+1}^z + S_j^z S_{j+1}^y) \right] \right\}, \quad (2)$$

where $\epsilon \equiv 1 + \frac{K}{2J}$ and N denotes the number of sites. The first line of Eq. (2) is the XXZ model, where the anisotropy parameter ϵ is determined by the ratio of Heisenberg J and Kitaev K interactions.

To examine the ordered state and phase transition under a field along the b ($\parallel y$)-axis, we add the Zeeman term $H_{\text{ext}} = -g\mu_B \sum_i \mathbf{h} \cdot \mathbf{S}_i$, where g is the g-factor and $\mathbf{h} = h \hat{y}$. As $S = 3/2$, $L = 1$, $J_{\text{eff}} = 1/2$ for the Co²⁺ ion, under no trigonal crystal field, we incorporate h using an isotropic Landé g-factor of $g = 4$ [30] and set $g\mu_B \equiv 1$. We employ the density matrix renormalization group (DMRG) method [36–38] for larger system sizes using the ITensor library [39]. The method is typically performed with a bond dimension larger than 1000 and a cutoff $\varepsilon < 10^{-10}$ meV [38, 40]. Unless otherwise noted, we assume periodic boundary conditions (PBCs), i.e. $\mathbf{S}_{N+1} = \mathbf{S}_1$. We also study the classical model to understand the impact of the bond-dependent interactions.

Zero field ordered phase - We first consider the zero-field ordered phase before turning to the field-induced transition. We may understand the form of the on-site magnetizations simply by analyzing the sign pattern of the Γ interaction in Eq. (2). In the ordered phase, due to a larger AFM Heisenberg interaction $J > 0$ and $\epsilon < 1$, we expect the moments $\mathbf{M}_j \equiv \langle \mathbf{S}_j \rangle$ with larger z -components to display Néel order, i.e. $M_j^z = (-1)^{j+1} m_z^0$. The Γ interaction then behaves as an effective staggered field $\sim \Gamma \sum_{j=1}^N (-1)^j [\cos(\pi j/2) (S_j^x - S_{j+1}^x) - \sin(\pi j/2) (S_j^y - S_{j+1}^y)]$, leading to a site-dependent g -tensor even in the absence of the external field. In the presence of the alternating component with a FM Kitaev interaction $K < 0$ and the Γ interactions, the moments have the following sign configurations

$$\mathbf{M}_j[\mathbf{h} = 0] = \begin{Bmatrix} \sqrt{2} \cos \left(\frac{2j+1}{4} \pi \right) m_x^0 \\ \sqrt{2} \cos \left(\frac{2j-1}{4} \pi \right) m_y^0 \\ (-1)^{j+1} m_z^0 \end{Bmatrix}, \quad (3)$$

where $m_x^0 = m_y^0$. From the classical analysis, m_x^0 and m_z^0 are given by

$$m_x^0 = \frac{\sqrt{8\Gamma^2 + (2J+K)^2} - (2J+K)}{4\Gamma} m_z^0, \quad m_z^0 = \frac{1}{2\sqrt{2}} \sqrt{1 + \frac{2J+K}{\sqrt{8\Gamma^2 + (2J+K)^2}}}. \quad (4)$$

The tilting angle is then given by $\phi = \arctan \left(\frac{\sqrt{2} m_x}{m_z} \right)$. As $\Gamma \rightarrow 0$, ϕ approaches 0, since $m_x^0 \rightarrow 0$. The detailed classical analysis is provided in the SM.

Note that the sign pattern of \mathbf{M}_j exhibits a four-sublattice periodicity. It is useful to group the sites j into a repeating four-site pattern: $4n+1$, $4n+2$, $4n+3$, $4n+4$, where n indexes the unit cell. Using this notation, the four-site pattern of M_n^z can be written as $M_n^z = (+m_z^0, -m_z^0, +m_z^0, -m_z^0)$ whereas $M_n^x = (-m_x^0, -m_x^0, +m_x^0, +m_x^0)$, as shown by the green arrows in Fig. 1(b) in the $z-x$ plane. M_j^y is determined by the four-fold screw rotation around the z -axis, i.e., $M_n^y = (+m_y^0, -m_y^0, -m_y^0, +m_y^0)$. The Γ interaction generates magnetizations in the $x-y$ plane that rotate by 90° as one moves along the z -axis, consistent with earlier studies employing a site-dependent g -tensor [15], with

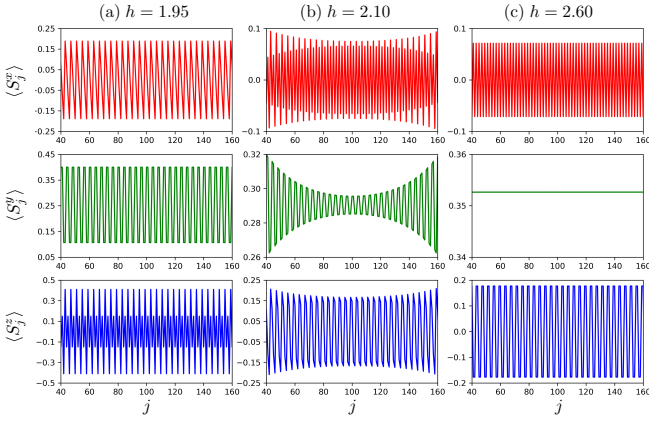


Fig. 2: DMRG results for the on-site magnetizations $\langle S_j^\gamma \rangle$ with $\gamma = x, y, z$ in the middle region of a $N = 200$ -site chain showing distinct four-sublattice patterns in three representative regions: (a) low-field ($h = 1.95$), (b) intermediate-field ($h = 2.10$), and (c) high-field ($h = 2.60$) regions.

the corresponding relations given in the SM. However, because the site-dependent g -tensor requires a finite external magnetic field, it does not accurately describe the ordered state at $h = 0$.

Transition under a magnetic field - We now consider the application of a magnetic field h applied along the y -axis (by symmetry, a field applied along the x -axis gives the same result). To obtain the critical fields where transitions occur, we study the magnetic susceptibility $\chi_h^e = -\partial^2 e_0 / \partial h^2$ where e_0 is the energy per site [38]. We adopt the values $J = 2.8$ meV and $\epsilon = 0.41$. The chosen J is slightly smaller than that inferred from analyses of field-induced phase transitions and the dispersion of spin excitations known as Zeeman ladders [12, 15, 41], but the phenomenological in-plane g -factor used in those earlier studies was also smaller than the isotropic g -factor inherent in the present microscopic model. Hereafter, all energies are in units of meV unless explicitly indicated. ϵ constrains $K = -3.3$, as $K = 2J(\epsilon - 1)$ from our Hamiltonian given by Eq. (2). Thus the system is described by a dominant FM Kitaev interaction and sub-dominant AFM Heisenberg interaction. Here we study the model with $\Gamma = 0.5$ –2 and present results for $\Gamma = 2$ in the main text. The qualitative behavior is insensitive to the precise value of Γ , and we show in the SM that the intermediate phase broadens as Γ increases.

The susceptibility χ_h^e in Fig. 3(a) shows a sharp feature at h_{c1} and h_{c2} denoted by purple and pink dashed lines, respectively. Strikingly, an intermediate region emerges between $h_{c1} < h < h_{c2}$ distinct from the low- and high-field phases. Fig. 2 shows the on-site magnetizations $\langle S_j^{x/y/z} \rangle$ in the middle region of a $N = 200$ -site chain for three representative field regions.

These magnetizations for the low-field regime, $h < h_{c1}$, take the form of sublattice magneti-

Field regime	M_n^x	M_n^y	M_n^z
$h = 0$	$(-, -, +, +)$	$(+, -, -, +)$	$(+, -, +, -)$
$h < h_{c1}$	$(-, -, +, +)$	$(+, +, +, +)$	$(+, -, +, -)$
$h > h_{c2}$	$(+, -, +, -)$	$(+, +, +, +)$	$(-, -, +, +)$

TABLE I: Sign structure of the four sublattice magnetizations M_n^x , M_n^y , and M_n^z for the low- and high-field ordered states. Note that the y -component sublattice structure present at $h = 0$ smoothly evolves into a uniform sign as the field h increases, but the magnitude of the sublattice pattern is shown in Fig. 2. As $h \rightarrow \infty$, the sublattice structure of \mathbf{M}_n remains unchanged, while the magnitude of the moments M_n^x and M_n^z approach zero.

zations, $M_n^x : (-m'_x, -m''_x, +m'_x, +m''_x)$, $M_n^z = (+m'_z, -m''_z, +m'_z, -m''_z)$, where positive constants m'_z, m''_z, m'_x, m''_x characterize the sublattice-dependent magnetization amplitudes, and $m'_{z/x} \neq m''_{z/x}$. The ground state is thus two-fold degenerate, and related by a two-fold screw rotation along the z -axis followed by time-reversal symmetry ($2_1 \times T$); see the SM.

For $h > h_{c2}$, the high-field phase exhibits a distinct alternating sign pattern of the sublattice magnetization as sketched in Fig. 1(c). In particular, the magnetizations take the form $M_n^x = (+m_x, -m_x, +m_x, -m_x)$, $M_n^z = (-m_z, -m_z, +m_z, +m_z)$, where m_z and m_x are positive constants. Notably, this alternating pattern is reversed relative to the ordered state below h_{c1} . Furthermore, since the magnitudes m_x and m_z are uniform across the sublattices, the ground state is nondegenerate; under the combined symmetry operation $2_1 \times T$, it maps onto itself. The sign structures of the four-sublattice \mathbf{M}_n^z components in the central unit cell are summarized in Table I. It is worth noting that the high-field phase is adiabatically connected to the fully polarized state, despite the nontrivial sublattice magnetizations. Classical spin-model calculations qualitatively reproduce the sublattice sign patterns (see the SM).

Intermediate-field phase - At the lower critical field h_{c1} , the DMRG calculation reveals a divergence in the second derivative of the ground state energy, signaling a second-order phase transition, as shown in Fig. 3(a). In contrast, the first derivative shows an anomaly at h_{c2} (inset of Fig. 3(a)), indicating a first-order transition.

To characterize the phases, we examine the spin-spin correlator $\langle S_1^y S_j^y \rangle$ as a function of distance j . As shown in Fig. 3(b), for $h < h_{c1}$ the correlator exhibits four-sublattice long-range magnetic order. In the intermediate phase $h_{c1} < h < h_{c2}$, the correlation decays exponentially at short distance, signaling a finite gap, and approaches a constant value set by the external field. Remarkably, this long-distance value at $j = 400$ drops sharply above h_{c2} , despite the further increase of the field applied along the y -axis, indicating distinct intermediate-field behavior.

To further highlight this transition, we plot the spin-spin correlator $\langle S_1^y S_{n=100}^y \rangle$ for the central unit cell ($\alpha =$

1–4, corresponding to $j = 401$ –404) as a function of h , shown in Fig. 3(c). It exhibits a clear jump at h_{c2} , corroborating the first-order nature of the transition inferred from the first derivative of the ground state energy.

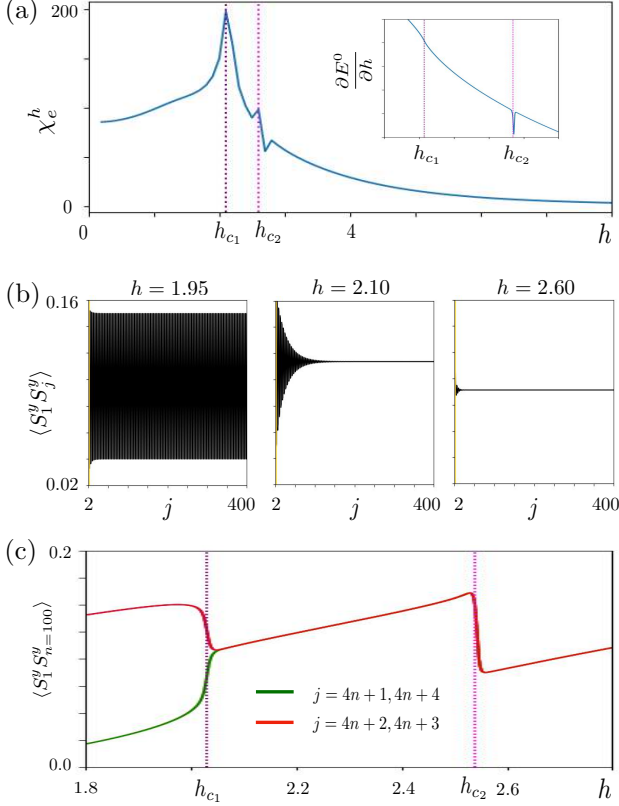


Fig. 3: DMRG results for $J = 2.8$, $K = -3.3$ and $\Gamma = 2$ as a function of the external field h with $N = 800$ sites. (a) Energy susceptibility χ_h^e where the purple and pink dashed lines mark the transitions at $h_{c1} = 2.03$ and $h_{c2} = 2.54$, respectively. The inset shows the first derivative of energy indicating the first order transition at h_{c2} . (b) Spin-spin correlator $\langle S_1^y S_j^y \rangle$ near the transitions as a function of j : $h(=1.95) < h_{c1}$, $h_{c1} < h(=2.10) < h_{c2}$, and $h(=2.60) > h_{c2}$. (c) Spin-spin correlator $\langle S_1^y S_{n=100}^y \rangle$ taken at the central unit cell with $\alpha = 1 - 4$, i.e., $j = 401 - 404$ as a function of the field. Note the sharp drop at h_{c2} , indicating the first order transition consistent with the first derivative of the ground state energy shown in the inset of (a).

Entanglement entropy and central charge – To understand the nature of the critical point h_{c1} , we investigate the spin-spin correlator and entanglement entropy. We compute the longitudinal correlator

$$\langle S_1^l S_j^l \rangle, j = 4n + 1, n = \{0, \dots, N_c\}, \quad (5)$$

where $S_j^l = \frac{1}{\sqrt{2}} \sin(\phi) (-S_j^x + S_j^y) + \cos(\phi) S_j^z$ for the sublattice $\alpha = 1$, ϕ is the angle from the c -axis as shown in Fig. 1(a), and N_c is the number of unit cells.

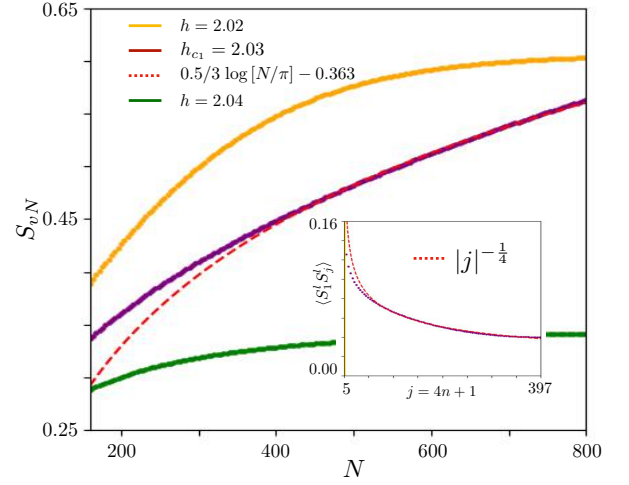


Fig. 4: DMRG results for the von Neumann entanglement entropy S_{vN} as a function of the chain size N for various values of h near h_{c1} . At $h = h_{c1}$, it scales as $\ln(N/\pi)$ with central charge $c = 1/2$, indicating the Ising critical point, whereas its deviation at other fields indicates a finite gap. The inset shows the longitudinal spin-spin correlator $\langle S_1^l S_j^l \rangle$ for the $\alpha = 1$ sublattice at $h = h_{c1}$, showing power-law behavior with the exponent $\eta = 1/4$.

We also determine the von Neumann entropy

$$S_{vN} = -\text{Tr}(\rho_{N'} \ln \rho_{N'}), \quad (6)$$

where $\rho_{N'}$ is the reduced density matrix of a subsystem of length N' [42, 43] for a chain of length N . We choose $N' = N/2 - 1$, i.e., the subsystem size is half the chain length. At critical points, where the spectral gap closes, S_{vN} scales as

$$S_{vN} \simeq \frac{c}{3} \ln \left[\frac{N}{\pi} \sin \left(\frac{\pi N'}{N} \right) \right] + c' \simeq \frac{c}{3} \ln \left[\frac{N}{\pi} \right] + c', \quad (7)$$

where c is the central charge of the underlying conformal field theory, and c' is a nonuniversal constant [43]. We show S_{vN} for h near h_{c1} in Fig. 4. From the purple curve at h_{c1} , we find the central charge $c = 0.5$. The inset shows $\langle S_1^l S_j^l \rangle$ given by Eq. (5) at h_{c1} . Notably, h_{c1} is a critical point where the longitudinal spin-spin correlator decays as a power law: $\langle S_1^l S_j^l \rangle \sim |j|^{-\eta}$ where $\eta = 0.25(1)$. This is consistent with the 2D Ising critical point [44, 45].

Summary and discussion – In summary, we have investigated the microscopic origin of the phenomenological site-dependent g -tensor introduced to explain unusual spin excitations and field-induced transitions in quasi-one-dimensional Co^{2+} chain materials such as $\text{BaCo}_2\text{V}_2\text{O}_8$. Within the JKT Hamiltonian, we have shown that the Γ interaction naturally alternates its sign across the four sublattices as a consequence of the $\pi/2$ screw-chain crystal structure. Surprisingly, the microscopic Hamiltonian reveals two distinct transitions under an external field. Our DMRG results establish that

the lower transition at h_{c1} is the Ising critical point, supported by the power-law decay of the spin-spin correlators and a central charge $c = 1/2$ extracted from the von Neumann entanglement entropy. In contrast, the upper transition at h_{c2} is first-order, characterized by a discontinuous jump in the spin-spin correlator. Furthermore, the width of the intermediate phase grows as Γ increases; see the SM for DMRG results with $\Gamma = 0.5, 1.5$. While we have uncovered a gapped intermediate phase, its precise nature remains to be clarified through future investigations.

Our analysis has focused on the idealized octahedral limit; however, real materials exhibit octahedral distortions that generate three additional interactions [32]. Given the symmetry constraints imposed by the four-fold screw axis, we expect the qualitative features of our results to remain robust, though the quantitative val-

ues of the critical fields will be modified. A systematic incorporation of these distortions represents a valuable direction for future study. More broadly, the current microscopic theory opens several future research avenues: extending the analysis to arbitrary field directions, examining finite-temperature signatures of the two transitions, and exploring related screw-chain systems where competing interactions may stabilize even richer quantum phases.

—
Acknowledgments - This work is supported by the NSERC Discovery Grant No. 2022-04601 and NSERC CREATE program No. 564506 - 21. H. Y. K. acknowledges support from the Canada Research Chairs Program No. CRC-2019-00147. This research was enabled in part by support provided by Compute Ontario, Calcul Québec, and the Digital Research Alliance of Canada.

-
- [1] J.-P. Renard, L.-P. Regnault, and M. Verdaguer, Haldane quantum spin chains, in *Magnetism: Molecules to Materials I: Models and Experiments*, edited by J. S. Miller and M. Drillon (Wiley-VCH, Weinheim, 2001) pp. 49–93.
 - [2] T. Giamarchi, *Quantum Physics in One Dimension*, International Series of Monographs on Physics, Vol. 121 (Clarendon Press, Oxford, 2004).
 - [3] H.-J. Mikeska and A. K. Kolezhuk, One-dimensional magnetism, in *Quantum Magnetism*, Lecture Notes in Physics, Vol. 645, edited by U. Schollwöck, J. Richter, D. J. J. Farnell, and R. F. Bishop (Springer, Berlin, 2004) pp. 1–83.
 - [4] A. W. Sandvik, Computational studies of quantum spin systems, in *AIP Conference Proceedings*, Vol. 1297 (American Institute of Physics, 2010) pp. 135–338, [arXiv:1101.3281](https://arxiv.org/abs/1101.3281).
 - [5] U. Schollwöck, The density-matrix renormalization group in the age of matrix product states, *Annals of Physics* **326**, 96 (2011).
 - [6] Y. Zhou, K. Kanoda, and T.-K. Ng, Quantum spin liquid states, *Reviews of Modern Physics* **89**, 025003 (2017), [arXiv:1607.03228](https://arxiv.org/abs/1607.03228).
 - [7] R. Wichmann and H. Müller-Buschbaum, Neue verbindungen mit srni2v2o8-struktur: Baco2v2o8 und bamg2v2o8, *Zeitschrift für Anorganische und Allgemeine Chemie* **534**, 153 (1986).
 - [8] Z. He, D. Fu, T. Kyômen, T. Taniyama, and M. Itoh, Crystal growth and magnetic properties of baco2v2o8, *Chemistry of Materials* **17**, 2924 (2005), <https://doi.org/10.1021/cm050760e>.
 - [9] Z. He, T. Taniyama, T. Kyômen, and M. Itoh, Field-induced order-disorder transition in the quasi-one-dimensional anisotropic antiferromagnet BaCo2V2O8, *Physical Review B* **72**, 172403 (2005).
 - [10] Z. He, T. Taniyama, and M. Itoh, Large magnetic anisotropy in the quasi-one-dimensional system BaCo2V2O8, *Applied Physics Letters* **88**, 132504 (2006).
 - [11] Y. Kawasaki, J. L. Gavilano, L. Keller, J. Schefer, N. B. Christensen, A. Amato, T. Ohno, Y. Kishimoto, Z. He, Y. Ueda, and M. Itoh, Magnetic structure and spin dynamics of the quasi-one-dimensional spin-chain antiferromagnet baco2v2o8, *Phys. Rev. B* **83**, 064421 (2011).
 - [12] S. Kimura, K. Okunishi, M. Hagiwara, K. Kindo, Z. He, T. Taniyama, M. Itoh, K. Koyama, and K. Watanabe, Collapse of magnetic order of the quasi one-dimensional ising-like antiferromagnet baco2v2o8 in transverse fields, *Journal of the Physical Society of Japan* **82**, 033706 (2013).
 - [13] S. K. Niesen, G. Kolland, M. Seher, O. Breunig, M. Vallador, M. Braden, B. Grenier, and T. Lorenz, Magnetic phase diagrams, domain switching, and quantum phase transition of the quasi-one-dimensional ising-like antiferromagnet baco2v2o8, *Phys. Rev. B* **87**, 224413 (2013).
 - [14] Y. Ideta, Y. Kawasaki, Y. Kishimoto, T. Ohno, Y. Michihiro, Z. He, Y. Ueda, and M. Itoh, ⁵¹V-NMR study of the quasi-one-dimensional antiferromagnet BaCo2V2O8, *Journal of the Korean Physical Society* **63**, 739 (2013).
 - [15] Q. Faure, S. Takayoshi, S. Petit, V. Simonet, S. Raymond, L.-P. Regnault, M. Boehm, J. S. White, M. Månsson, C. Rüegg, *et al.*, Topological quantum phase transition in the ising-like antiferromagnetic spin chain baco2v2o8, *Nature Physics* **14**, 716 (2018).
 - [16] C.-M. Halati, Z. Wang, T. Lorenz, C. Kollath, and J.-S. Bernier, Repulsively bound magnon excitations of a spin-1 2 xxz chain in a staggered transverse field, *Physical Review B* **108**, 224429 (2023).
 - [17] M. Månsson, K. Prša, J. Sugiyama, T. Goko, C. Baines, A. Amato, F. L. Pratt, Z. He, and M. Itoh, Microscopic magnetic nature of the quasi-one-dimensional antiferromagnet baco2v2o8, *Physica Procedia* **30**, 146 (2012).
 - [18] Y. Kawasaki, Y. Ideta, Y. Kishimoto, T. Ohno, Y. Michihiro, Z. He, Y. Ueda, and M. Itoh, Antiferromagnetic state in the quasi-one-dimensional baco2v2o8: ⁵¹v-nmr study on a single crystal, in *Journal of the Physical Society of Japan Conference Proceedings*, Vol. 3 (2014) p. 014001.
 - [19] Z. Wang, M. Schmidt, A. Günther, N. M. Bruckner, M. Baenitz, Y. Skourski, J. Wosnitza, H. Berger, V. Zapf, B. Normand, Z. Weichselbaum, I. Affleck, F. Faisan, P. Lejay, and B. Lake, Quantum criticality of an ising-like spin-1/2 antiferromagnetic chain in a transverse mag-

- netic field, [Physical Review Letters](#) **120**, 207205 (2018).
- [20] Q. Faure, S. Takayoshi, S. Petit, B. Lake, S. Raymond, M. Boehm, P. Lejay, V. Simonet, T. Giamarchi, and B. Grenier, From confined spinons to emergent fermions: Observing the spinon confinement–deconfinement crossover in the ising-like chain $\text{BaCo}_2\text{V}_2\text{O}_8$, [Physical Review Letters](#) **123**, 027204 (2019).
- [21] Q. Faure, S. Takayoshi, B. Grenier, S. Petit, S. Raymond, M. Boehm, P. Lejay, T. Giamarchi, and V. Simonet, Solitonic excitations in the ising anisotropic chain $\text{BaCo}_2\text{V}_2\text{O}_8$ under large transverse magnetic field, [Physical Review Research](#) **3**, 043227 (2021), [arXiv:2107.02487 \[cond-mat.str-el\]](#).
- [22] Y. Cui, H. Zou, N. Xi, Z. He, Y. Yang, L. Shu, G. Zhang, Z. Hu, T. Chen, R. Yu, *et al.*, Quantum criticality of the ising-like screw chain antiferromagnet $\text{SrCo}_2\text{V}_2\text{O}_8$ in a transverse magnetic field, [Phys. Rev. Lett.](#) **123**, 067203 (2019).
- [23] A. Okutani, H. Onishi, S. Kimura, T. Takeuchi, T. Kida, M. Mori, A. Miyake, M. Tokunaga, K. Kindo, and M. Hagiwara, Spin excitations of the $s = 1/2$ one-dimensional ising-like antiferromagnet $\text{BaCo}_2\text{V}_2\text{O}_8$ in transverse magnetic fields, [Journal of the Physical Society of Japan](#) **90**, 044704 (2021).
- [24] H. Zou, Y. Cui, X. Wang, Z. Zhang, J. Yang, G. Xu, A. Okutani, M. Hagiwara, M. Matsuda, G. Wang, *et al.*, E 8 spectra of quasi-one-dimensional antiferromagnet $\text{BaCo}_2\text{V}_2\text{O}_8$ under transverse field, [Physical review letters](#) **127**, 077201 (2021).
- [25] T. Giamarchi and H. Schulz, Theory of spin-anisotropic electron-electron interactions in quasi-one-dimensional metals, [Journal de Physique](#) **49**, 819 (1988).
- [26] P. Lecheminant, A. O. Gogolin, and A. A. Nersisyan, Criticality in selfdual sine-Gordon models, [Nucl. Phys. B](#) **639**, 502 (2002), [arXiv:cond-mat/0203294](#).
- [27] H. Liu and G. Khaliullin, Pseudospin exchange interactions in d^7 cobalt compounds: Possible realization of the kitaev model, [Phys. Rev. B](#) **97**, 014407 (2018).
- [28] R. Sano, Y. Kato, and Y. Motome, Kitaev-Heisenberg Hamiltonian for high-spin d^7 Mott insulators, [Phys. Rev. B](#) **97**, 014408 (2018).
- [29] J. G. Rau, E. K.-H. Lee, and H.-Y. Kee, Generic Spin Model for the Honeycomb Iridates beyond the Kitaev Limit, [Phys. Rev. Lett.](#) **112**, 077204 (2014).
- [30] H. Liu, J. c. v. Chaloupka, and G. Khaliullin, Kitaev Spin Liquid in 3d Transition Metal Compounds, [Phys. Rev. Lett.](#) **125**, 047201 (2020).
- [31] X. Liu and H.-Y. Kee, Non-Kitaev versus Kitaev honeycomb cobaltates, [Phys. Rev. B](#) **107**, 054420 (2023).
- [32] D. Churchill and H.-Y. Kee, Transforming from kitaev to disguised ising chain: Application to Co_2O_6 , [Physical Review Letters](#) **133**, 056703 (2024).
- [33] Y. Matsuda, T. Shibauchi, and H.-Y. Kee, Kitaev quantum spin liquids, [Rev. Mod. Phys.](#) **97**, 045003 (2025).
- [34] S. M. Winter, Magnetic couplings in edge-sharing high-spin d^7 compounds, [Journal of Physics: Materials](#) **5**, 045003 (2022).
- [35] I. Rousochatzakis, N. Perkins, Q. Luo, and H.-Y. Kee, [Reports on Progress in Physics](#) **87**, 026502 (2024).
- [36] S. R. White, Density matrix formulation for quantum renormalization groups, [Physical review letters](#) **69**, 2863 (1992).
- [37] U. Schollwöck, The density-matrix renormalization group in the age of matrix product states, [Annals of physics](#) **326**, 96 (2011).
- [38] M. Bhullar, H. Xu, and H.-Y. Kee, Field-induced ordered phases in anisotropic spin-1 2 kitaev chains, [Physical Review B](#) **111**, 104439 (2025).
- [39] M. Fishman, S. White, and E. M. Stoudenmire, The itensor software library for tensor network calculations, [SciPost Physics Codebases](#) , 004 (2022).
- [40] E. S. Sørensen, J. Gordon, J. Riddell, T. Wang, and H.-Y. Kee, Field-induced chiral soliton phase in the Kitaev spin chain, [Phys. Rev. Res.](#) **5**, L012027 (2023).
- [41] B. Grenier, S. Petit, V. Simonet, E. Canévet, L.-P. Regnault, S. Raymond, B. Canals, C. Berthier, and P. Lejay, Longitudinal and transverse zeeman ladders in the ising-like chain antiferromagnet $\text{BaCo}_2\text{V}_2\text{O}_8$, [Phys. Rev. Lett.](#) **114**, 017201 (2015).
- [42] E. S. Sørensen, A. Catuneanu, J. S. Gordon, and H.-Y. Kee, Heart of Entanglement: Chiral, Nematic, and Incommensurate Phases in the Kitaev-Gamma Ladder in a Field, [Phys. Rev. X](#) **11**, 011013 (2021).
- [43] A. Mitra, S. Paul, and S. C. L. Srivastava, Quantum criticality and universality in the stationary state of the long-range kitaev model, [Phys. Rev. B](#) **111**, 104308 (2025).
- [44] E. W. Montroll, R. B. Potts, and J. C. Ward, Correlations and spontaneous magnetization of the two-dimensional ising model, [Journal of Mathematical Physics](#) **4**, 308 (1963).
- [45] T. T. Wu, B. M. McCoy, C. A. Tracy, and E. Barouch, Spin-spin correlation functions for the two-dimensional ising model: Exact theory in the scaling region, [Physical Review B](#) **13**, 316 (1976).

Supplementary Material for “Microscopic Theory Revealing Dual Field-Induced Transitions in Spin- $\frac{1}{2}$ Screw-Chain Magnets”

Mandev Bhullar,¹ Philip Richard,¹ and Hae-Young Kee^{1,2,*}

¹*Department of Physics, University of Toronto, Ontario, Canada M5S 1A7*

²*Canadian Institute for Advanced Research, CIFAR Program in Quantum Materials, Toronto, Ontario, Canada, M5G 1M1*
(Dated: December 11, 2025)

I. DERIVATION OF MICROSCOPIC HAMILTONIAN

In this section, we identify the origin of the sign structure appearing in the Γ term of the Hamiltonian H given by Eq. (1) in the main text. Focusing on a single bond at a time, we define the local axes as pointing towards the oxygen atoms of the octahedral cage. Then, for two edge-sharing octahedra, two of those axes will lie in the edge-sharing plane, while the remaining one will be perpendicular to it. In the case of the first bond, the y - and z -axes are in the shared plane while the x -axis is pointing out of the page, as shown in Fig. S1.

It is then known that Co^{2+} ions in such an environment give rise to an effective nearest-neighbour $J_{\text{eff}} = 1/2$ exchange Hamiltonian of the form [1–5]

$$H_{ij} = J\mathbf{S}_i \cdot \mathbf{S}_j + K S_i^\gamma S_j^\gamma + \Gamma (S_i^\alpha S_j^\beta + S_i^\beta S_j^\alpha), \quad (\text{S1})$$

where α, β are the two in-plane directions, while γ is the out-of-plane one. So, for the first bond, we have

$$H_{12} = J\mathbf{S}_1 \cdot \mathbf{S}_2 + K S_1^x S_2^x + \Gamma (S_1^y S_2^z + S_1^z S_2^y). \quad (\text{S2})$$

If we look at the next bond, because of the screw structure, the shared edge of the two octahedra now lies in the $x - z$ plane while the y -axis points out of the plane. So carrying out the derivation of Eq. (S1) would yield the same form, but now with $x \leftrightarrow y$, so the resulting bond Hamiltonian would be

$$H_{23} = J\mathbf{S}_2 \cdot \mathbf{S}_3 + K S_2^y S_3^y + \Gamma (S_2^x S_3^z + S_2^z S_3^x). \quad (\text{S3})$$

Moving on to the third bond, the shared edge is again in the $y - z$ plane, but the corresponding local axes are now z and $-y$. So, the Hamiltonian for this bond would be the same as Eq. (S2), but now the extra minus sign is accounted for by sending $S^y \rightarrow -S^y$. This is then absorbed in the Γ factor which yields

$$H_{34} = J\mathbf{S}_3 \cdot \mathbf{S}_4 + K S_3^x S_4^x - \Gamma (S_3^y S_4^z + S_3^z S_4^y). \quad (\text{S4})$$

Similarly for the last bond, the local axes are z and $-x$, and so the resulting Hamiltonian is

$$H_{41} = J\mathbf{S}_4 \cdot \mathbf{S}_1 + K S_4^y S_1^y - \Gamma (S_4^x S_1^z + S_4^z S_1^x). \quad (\text{S5})$$

Putting Eqs. (S2)-(S5) together and incorporating the sublattice dependence leads to the Hamiltonian given by Eq. (2) in the main text.

II. CLASSICAL ANALYSIS

We first note that the classical analog of the model with PBCs given by Eq. (2) in the main text under a field h applied along the y -axis may be written as

$$\begin{aligned} H_{\text{cl}} = N_c \bigg[& \left(J + \frac{K}{2} \right) [S_1^x S_2^x + S_1^y S_2^y + S_2^x S_3^x + S_2^y S_3^y + S_3^x S_4^x + S_3^y S_4^y + S_4^x S_1^x + S_4^y S_1^y] \\ & + J [S_1^z S_2^z + S_2^z S_3^z + S_3^z S_4^z + S_4^z S_1^z] + \frac{K}{2} [S_1^x S_2^x - S_1^y S_2^y - S_2^x S_3^x + S_2^y S_3^y + S_3^x S_4^x - S_3^y S_4^y - S_4^x S_1^x + S_4^y S_1^y] \\ & + \Gamma [S_1^y S_2^z + S_1^z S_2^y + S_2^y S_3^z + S_2^z S_3^y - S_3^y S_4^z - S_3^z S_4^y - S_4^y S_1^z - S_4^z S_1^y] - h [S_1^y + S_2^y + S_3^y + S_4^y] \bigg], \quad (\text{S6}) \end{aligned}$$

* hy.kee@utoronto.ca

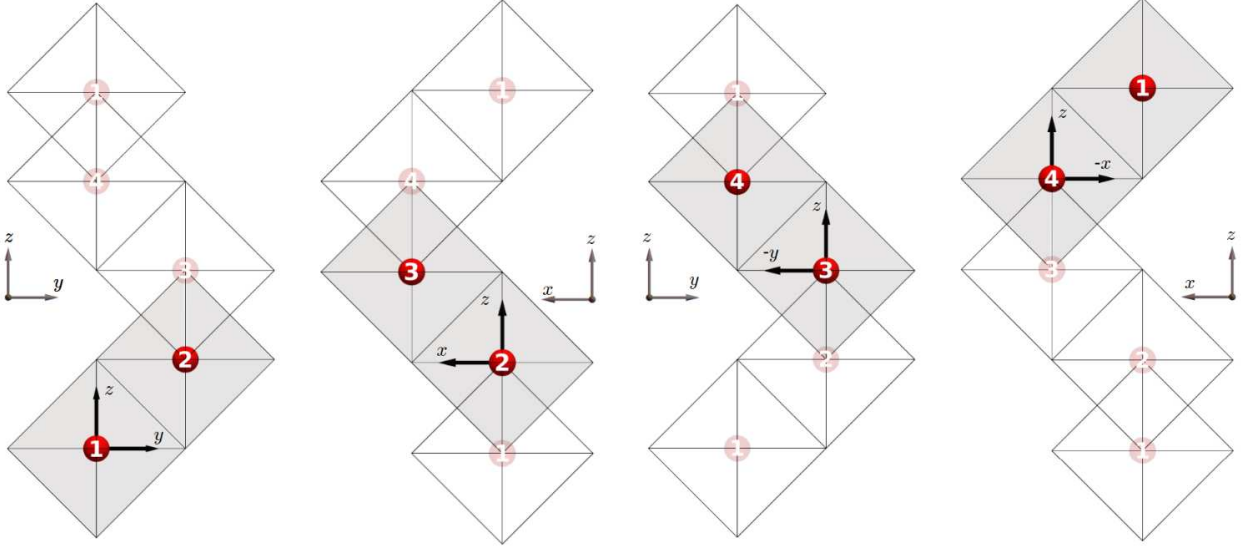


Fig. S1: Choice of local axes used in the derivation of the JKT exchange Hamiltonian. For each bond, indicated in grey, the local axes are those pointing towards the ligand atoms of the shared edge. Because of the screw structure, the corresponding axes change from one bond to the next. This is reflected in the sign structure in the full Hamiltonian.

where \mathbf{S}_j ($j = 1, 2, 3, 4$) are four spins in a unit cell, and N_c is the number of unit cells.

A. Zero Field $h = 0$

As discussed in the main text, at zero field, due to a larger AFM Heisenberg interaction $J > 0$ and anisotropy parameter $\epsilon < 1$, we expect the moments $\mathbf{M}_j \equiv \langle \mathbf{S}_j \rangle$ with larger z -components to display Néel order. This implies we can take the ansatz where $S_1^z = +m_z^0$, $S_2^z = -m_z^0$, $S_3^z = +m_z^0$, $S_4^z = -m_z^0$. Using this ansatz, we aim to minimize the classical Hamiltonian given by Eq. (S6) under the constraint $(S_j^x)^2 + (S_j^y)^2 + (m_z^0)^2 = S^2$ with $S = 1/2$. This is the strong condition of the Luttinger-Tisza method to find the optimal spin configuration that minimizes the classical energy [6, 7]. We define the function

$$\begin{aligned} \mathcal{G} &= H_{cl}(h=0) - N_c \lambda \sum_{j=1}^4 (S^2 - (S_j^x)^2 - (S_j^y)^2 - (m_z^0)^2) \\ &= N_c \left\{ -4J(m_z^0)^2 + (J+K)S_1^x S_2^x + JS_1^y S_2^y - \Gamma m_z^0 (S_1^y - S_2^y) + (J+K)S_2^y S_3^y + JS_2^x S_3^x + \Gamma m_z^0 (S_2^x - S_3^x) \right. \\ &\quad + (J+K)S_3^x S_4^x + JS_3^y S_4^y + \Gamma m_z^0 (S_3^y - S_4^y) + (J+K)S_4^y S_1^y + JS_4^x S_1^x - \Gamma m_z^0 (S_4^x - S_1^x) \\ &\quad \left. - \lambda (4S^2 - (S_1^x)^2 - (S_1^y)^2 - (S_2^x)^2 - (S_2^y)^2 - (S_3^x)^2 - (S_3^y)^2 - (S_4^x)^2 - (S_4^y)^2 - 4(m_z^0)^2) \right\}, \quad (\text{S7}) \end{aligned}$$

and set the constraints

$$\frac{\partial \mathcal{G}}{\partial S_j^x} = 0, \quad \frac{\partial \mathcal{G}}{\partial S_j^y} = 0, \quad \frac{\partial \mathcal{G}}{\partial m_z^0} = 0, \quad \frac{\partial \mathcal{G}}{\partial \lambda} = 0. \quad (\text{S8})$$

In solving the system of equations given by Eq. (S8) that minimize the classical energy E_{cl} , we find the following solution:

$$S_j^x = \begin{cases} -m_x^0, & j=1 \\ -m_x^0, & j=2 \\ +m_x^0, & j=3 \\ +m_x^0, & j=4 \end{cases}, \quad S_j^y = \begin{cases} +m_y^0, & j=1 \\ -m_y^0, & j=2 \\ -m_y^0, & j=3 \\ +m_y^0, & j=4 \end{cases}, \quad S_j^z = \begin{cases} +m_z^0, & j=1 \\ -m_z^0, & j=2 \\ +m_z^0, & j=3 \\ -m_z^0, & j=4 \end{cases}, \quad (\text{S9})$$

where

$$m_x^0 = m_y^0 \equiv \frac{\sqrt{8\Gamma^2 + (2J + K)^2} - (2J + K)}{4\Gamma} m_z^0, \text{ and } m_z^0 \equiv \frac{1}{2\sqrt{2}} \sqrt{1 + \frac{2J + K}{\sqrt{8\Gamma^2 + (2J + K)^2}}}. \quad (\text{S10})$$

Because we are at $h = 0$, the time-reversal of this solution, i.e. $\mathbf{S}_j \rightarrow -\mathbf{S}_j$, is also at a minimum.

In the limit $\Gamma \rightarrow 0$, we find that $m_x^0 \rightarrow 0$, and $m_z^0 \rightarrow 1/2$, which confirms on the classical level that the Γ interaction is responsible for the finite x - and y -components of the moment. The tilt angle of the spins from the z -axis is therefore

$$\phi_{\text{cl}} = \arctan\left(\frac{\sqrt{2}m_x^0}{m_z^0}\right) = \arctan\left(\frac{\sqrt{8\Gamma^2 + (2J + K)^2} - (2J + K)}{2\sqrt{2}\Gamma}\right). \quad (\text{S11})$$

As a reference, if we plug in the parameters used in the main text, $J = 2.8$, $K = -3.3$ and a small value of $\Gamma = 0.5$, this gives $\phi_{\text{cl}} \approx 15^\circ$, while the DMRG gives a smaller angle due to quantum fluctuations. We also note that the above expression is a monotonically increasing function of Γ , which means that increasing the strength of this interaction gives a larger tilt angle. It also affects the critical field strengths and the window of the field-induced intermediate phase as shown below.

B. Under Field Applied Along y -Axis $h > 0$

Under a field applied along the y -axis $h > 0$, assuming no broken translational symmetry, the classical energy with the constraint $(S_j^x)^2 + (S_j^y)^2 + (S_j^z)^2 = S^2$ with $S = 1/2$ is written as

$$\begin{aligned} \mathcal{F}(h) &= H_{\text{cl}}(h) - N_c \lambda \sum_{j=1}^4 (S^2 - (S_j^x)^2 - (S_j^y)^2 - (S_j^z)^2) \\ &= N_c \left[\left(J + \frac{K}{2} \right) [S_1^x S_2^x + S_1^y S_2^y + S_2^x S_3^x + S_2^y S_3^y + S_3^x S_4^x + S_3^y S_4^y + S_4^x S_1^x + S_4^y S_1^y] \right. \\ &\quad + J [S_1^z S_2^z + S_2^z S_3^z + S_3^z S_4^z + S_4^z S_1^z] + \frac{K}{2} [S_1^x S_2^x - S_1^y S_2^y - S_2^x S_3^x + S_2^y S_3^y + S_3^x S_4^x - S_3^y S_4^y - S_4^x S_1^x + S_4^y S_1^y] \\ &\quad + \Gamma [S_1^y S_2^z + S_1^z S_2^y + S_2^x S_3^z + S_2^z S_3^x - S_3^y S_4^z - S_3^z S_4^y - S_4^x S_1^z - S_4^z S_1^x] + h [S_1^y + S_2^y + S_3^y + S_4^y] \\ &\quad \left. - \lambda [4S^2 - (S_1^x)^2 - (S_1^y)^2 - (S_1^z)^2 - (S_2^x)^2 - (S_2^y)^2 - (S_2^z)^2 - (S_3^x)^2 - (S_3^y)^2 - (S_3^z)^2 - (S_4^x)^2 - (S_4^y)^2 - (S_4^z)^2] \right]. \end{aligned} \quad (\text{S12})$$

We then set the constraints as follows:

$$\frac{\partial \mathcal{F}}{\partial S_j^x} = 0, \frac{\partial \mathcal{F}}{\partial S_j^y} = 0, \frac{\partial \mathcal{F}}{\partial S_j^z} = 0, \frac{\partial \mathcal{F}}{\partial \lambda} = 0. \quad (\text{S13})$$

We solve the system of equations given by Eq. (S13) numerically as a function of h , with the initial guess of our calculation being the first of the zero field configurations given by Eq. (S9). The ground state energy E_{cl} is found by substituting the resulting configurations into Eq. (S6). Fig. S2 shows these configurations as a function of h for different values of Γ . For low and high fields, the classical result is qualitatively similar to what is seen in DMRG. However, it is not able to fully capture the behaviour near the transition.

III. RELATION TO SITE-DEPENDENT g -TENSOR

The model given by Eq. (2) in the main text is related to the site-dependent g -tensor previously proposed for $\text{BaCo}_2\text{V}_2\text{O}_8$ via the magnetization structure found in the high-field state, which as discussed in the main text vanishes and completely aligns with the field in the limit $h \rightarrow \infty$. The phenomenological model previously proposed for $\text{BaCo}_2\text{V}_2\text{O}_8$ for a field applied along the crystallographic b -direction, i.e. y -direction, is given by Eq. (1) of Faure et. al [8], which includes a weak-interchain coupling term $J' \sum_j \sum_{\mu, \nu (\mu \neq \nu)} S_{j, \mu}^z S_{j, \nu}^z$, where μ, ν index the chains and j indexes the sites. Given that we have not included interchain coupling in this work, we set this term to zero and

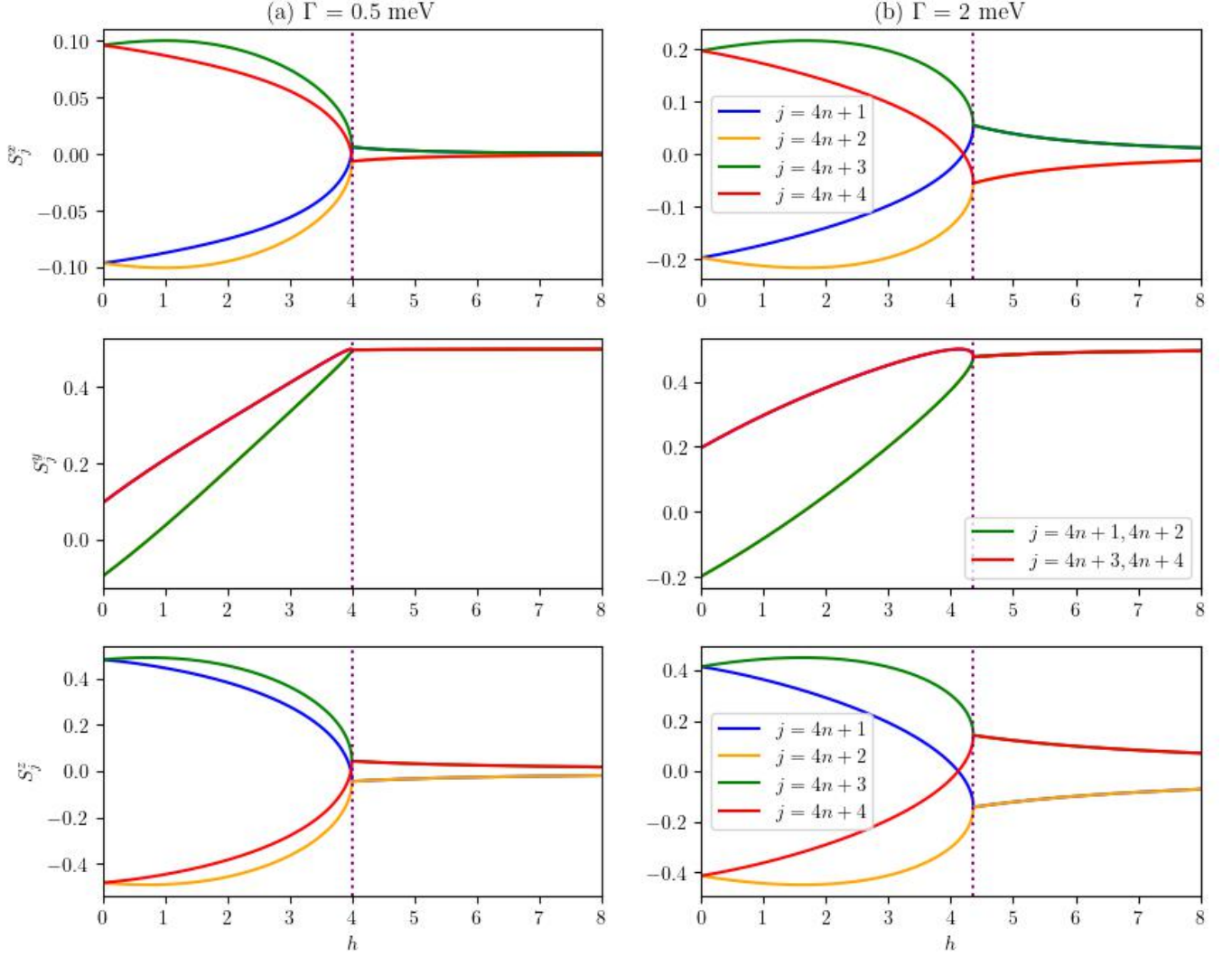


Fig. S2: The classical spins $S_j^{x/y/z}$, $j = 4n + 1, 4n + 2, 4n + 3, 4n + 4$ within a unit cell of the JKT model versus a field applied along the y -axis h for $J = 2.8$, $K = -3.3$ and various Γ . The purple dashed line marks the transition point $h_{c,cl}$ from the classical ordered phase to the high-field state. Here, we assume no broken translational symmetry. (a) $\Gamma = 0.5$, $h_{c,cl} = 4.00$. (b) $\Gamma = 2$, $h_{c,cl} = 4.36$.

write their phenomenological model as

$$\mathcal{H} = J \sum_j [\epsilon(S_j^x S_{j+1}^x + S_j^y S_{j+1}^y) + S_j^z S_{j+1}^z] - h \hat{\mathbf{y}} \cdot \sum_j \tilde{G}_j \mathbf{S}_j, \quad (\text{S14})$$

where $\mathbf{S}_j = [S_j^x \ S_j^y \ S_j^z]^T$. The first term of Eq. (S14) is the XXZ model, similar to the first term of our model given by Eq. (2) in the main text. When the external field is applied along the y -axis, the relevant components are \tilde{G}_j^{yx} , \tilde{G}_j^{yy} and \tilde{G}_j^{yz} , which has been proposed to have site-dependence of the form [8, 9]

$$\tilde{G}_j^{yx} = g_{yx}(-1)^{j+1}, \quad \tilde{G}_j^{yy} = g_{yy}, \quad \tilde{G}_j^{yz} = g_{yz} \cos\left(\frac{2j+1}{4}\pi\right). \quad (\text{S15})$$

Note that our magnetization structure in the high-field regime has the same sign structure as Eq. (S15),

$$\langle S_j^x \rangle = [m_x(h)](-1)^{j+1}, \quad \langle S_j^y \rangle = [m_y(h)], \quad \langle S_j^z \rangle = [m_z(h)] \cos\left(\frac{2j+1}{4}\pi\right), \quad (\text{S16})$$

where the field-dependent functions $m_x(h)$, $m_y(h)$, $m_z(h)$ are positive and satisfy the limits $m_x(h \rightarrow \infty) \rightarrow 0$,

$m_z(h \rightarrow \infty) \rightarrow 0$ and $m_y(h \rightarrow \infty) \rightarrow 0.5$. Thus, the Γ interaction gives rise to an effective g -tensor that corresponds to the site-dependent phenomenological g -tensor that was previously used. However, it is important to note that its effects are different from the external field as it generates the intermediate phase via the interplay with the external field.

IV. SEPARATION OF h_{c1} AND h_{c2} VS Γ

We find from DMRG that a larger Γ interaction separates the two critical fields h_{c1} and h_{c2} , but both values decrease as Γ increases. We show that this is the case below with the susceptibility $\chi_h^e = -\partial^2 e_0 / \partial h^2$ for $\Gamma = 0.5, 1.5, 2$, found with $N = 800$ sites. When $\Gamma = 0.5$, we find that $h_{c1} \simeq 2.95$ and $h_{c2} \simeq 3.12$ (so that $h_{c2} - h_{c1} \simeq 0.17$). When $\Gamma = 1.5$, we find that $h_{c1} \simeq 2.43$ and $h_{c2} \simeq 2.77$ (so that $h_{c2} - h_{c1} \simeq 0.34$). We compare these values with those of $\Gamma = 2$, where $h_{c1} = 2.03$ and $h_{c2} = 2.54$ (so that $h_{c2} - h_{c1} = 0.51$), as discussed in the main text.

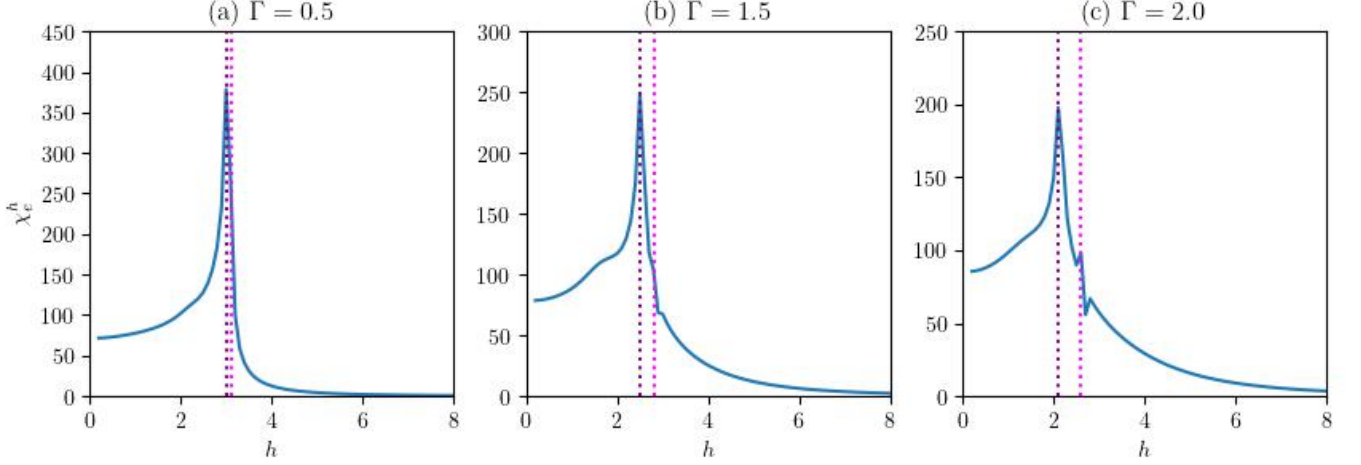


Fig. S3: DMRG results for the energy susceptibility χ_h^e as a function of the external field h for various Γ values with $J = 2.8$, $K = -3.3$ and $N = 800$ sites. The purple dashed lines mark h_{c1} and the pink dashed lines mark h_{c2} . (a) $\Gamma = 0.5$, $h_{c1} = 2.95$, $h_{c2} = 3.12$. (b) $\Gamma = 1.5$, $h_{c1} = 2.43$, $h_{c2} = 2.77$. (c) $\Gamma = 2$, $h_{c1} = 2.03$, $h_{c2} = 2.54$.

V. SYMMETRY ANALYSIS

While adding a field applied along the y -axis breaks both time-reversal and screw-axis symmetries, the composition of a 2-fold screw-axis and time-reversal, $2_1 \times T$, is still a symmetry. This action has the effect of sending $j \rightarrow j + 2$ and $S^z \rightarrow -S^z$, which one can verify leaves the Hamiltonian unchanged. However, the ground state in the low-field phase below h_{c1} is not invariant under this transformation. Indeed, at small field, the ground state has a magnetization configuration given by

$$M_x = (-m'_x, -m''_x, +m''_x, +m'_x) \quad M_y = (m'_y, m''_y, m''_y, m'_y) \quad M_z = (+m'_z, -m''_z, +m''_z, -m'_z), \quad (\text{S17})$$

where $m'_z, m''_z, m'_x, m''_x > 0$, and m'_y, m''_y respectively have negative and positive sign at very low field but continuously evolve until both become positive after a certain field strength. Applying this symmetry to the state gives a new magnetization pattern:

$$M_x = (+m''_x, +m'_x, -m'_x, -m''_x) \quad M_y = (m''_y, m'_y, m'_y, m''_y) \quad M_z = (-m''_z, +m'_z, -m'_z, +m''_z). \quad (\text{S18})$$

Hence, we have two different yet degenerate states.

On the other hand, in the high-field phase, the magnetization pattern is instead given by

$$M_x = (+m_x, -m_x, +m_x, -m_x) \quad M_y = (+m_y, +m_y, +m_y, +m_y) \quad M_z = (-m_z, -m_z, +m_z, +m_z). \quad (\text{S19})$$

If we now apply the $2_1 \times T$ on this state, we see that we end up with the same state, hence we have a unique ground state. From the DMRG calculations, we find that the degeneracy of the low-field phase is lifted at h_{c1} when the

system starts to evolve from one configuration to the next in the intermediate phase.

-
- [1] J. G. Rau, E. K.-H. Lee, and H.-Y. Kee, Generic Spin Model for the Honeycomb Iridates beyond the Kitaev Limit, [Phys. Rev. Lett. **112**, 077204 \(2014\)](#).
 - [2] H. Liu and G. Khaliullin, Pseudospin exchange interactions in d^7 cobalt compounds: Possible realization of the kitaev model, [Phys. Rev. B **97**, 014407 \(2018\)](#).
 - [3] R. Sano, Y. Kato, and Y. Motome, Kitaev-Heisenberg Hamiltonian for high-spin d^7 Mott insulators, [Phys. Rev. B **97**, 014408 \(2018\)](#).
 - [4] D. Churchill and H.-Y. Kee, Transforming from kitaev to disguised ising chain: Application to conb 2 o 6, [Physical Review Letters **133**, 056703 \(2024\)](#).
 - [5] Y. Matsuda, T. Shibauchi, and H.-Y. Kee, Kitaev quantum spin liquids, [Rev. Mod. Phys. **97**, 045003 \(2025\)](#).
 - [6] J. Luttinger and L. Tisza, Theory of dipole interaction in crystals, [Physical Review **70**, 954 \(1946\)](#).
 - [7] D. Litvin, The luttinger-tisza method, [Physica **77**, 205 \(1974\)](#).
 - [8] Q. Faure, S. Takayoshi, S. Petit, V. Simonet, S. Raymond, L.-P. Regnault, M. Boehm, J. S. White, M. Månsson, C. Rüegg, *et al.*, Topological quantum phase transition in the ising-like antiferromagnetic spin chain baco2v2o8, [Nature Physics **14**, 716 \(2018\)](#).
 - [9] S. Kimura, K. Okunishi, M. Hagiwara, K. Kindo, Z. He, T. Taniyama, M. Itoh, K. Koyama, and K. Watanabe, Collapse of magnetic order of the quasi one-dimensional ising-like antiferromagnet baco2v2o8 in transverse fields, [Journal of the Physical Society of Japan **82**, 033706 \(2013\)](#).